Supported ionic liquid water sorbent for high throughput desalination and drying

Supported ionic liquid water sorbent for high throughput desalination and drying

Ahmed A. Askalany[a,b], Angelo Freni[c], Giulio Santori[a,*]

[a] *The University of Edinburgh, School of Engineering, Institute for Materials and Processes, Sanderson Building, The King's Buildings, Mayfield Road, EH9 3BF Edinburgh, Scotland, UK*
[b] *Mechanical Engineering Department, Faculty of Industrial Education, Sohag University, Sohag, 82524, Egypt*
[c] *Consiglio Nazionale delle Ricerche, Istituto di Chimica dei Composti Organometallici (CNR-ICCOM) Via G. Moruzzi, 1, 56124, Pisa, Italy*

Corresponding Author: Dr. Giulio Santori
g.santori@ed.ac.uk
Tel. +44 (0)131 651 9043
Fax +44 (0)131 650 6551

ABSTRACT: The composite material 1-ethyl-3-methylimidazolium methanesulfonate ionic liquid in Syloid AL-1FP silica shows unprecedented water vapor sorption equilibrium properties. Equilibrium data were recorded at different loads of ionic liquid in the silica support (from 1.8%w to 60%w). At loadings >1.8%w, all the composites show type 3 isotherm, therefore conserving the vapor-liquid equilibrium of the bulk ionic liquid/water binary system but with increased dependence between temperature and water adsorbed. This feature makes this composite material particularly suitable for thermally-driven technologies. The composite 60%w 1-ethyl-3-methylimidazolium methanesulfonate ionic liquid in 40%w Syloid AL-1FP silica shifts the performance of sorption desalination and drying processes at the unprecedented working capacity of 0.46 $g_{water}/g_{sorbent}$ (desalination) and 0.82 $g_{water}/g_{sorbent}$ (drying).

1.Introduction

The increase in world population and energy need of both developed and developing countries contrasts the shortage of conventional resources and requires a more equitable distribution [1]. Energy available per capita is deemed to decrease in the next decades, hindering the quality of life that most of the technologically advanced countries have. Energy efficient processes and devices, utilization of primary energy sources which were discarded few years ago and sustained investment on renewable energy are nowadays part of the sustainable development roadmaps of many countries. Renewable and waste low-grade heat can contribute to the future primary energy portfolio as testified by recent intensification of research and development on technologies driven by heat below 100°C. Among these technologies, temperature swing sorption (TSS) systems, that make use of sorption materials or fluids, show viable performance [2-5]. TSS has been proposed to obtain diverse useful effects such as heat transformation and long term storage [6-10], desalination [11, 12], drying [13, 14] and in many separation processes [15]. The term sorption is here intentionally kept general and indicates both adsorption (sorption in a porous solid material) and absorption (sorption in a liquid solvent). In all cases sorption indicates the presence of a bond between the sorbent and the sorbate which in many applications is water. This is the case of sorption drying and desalination but also of many closed systems such as cooling, heating and heat storage where water can enable performance which rule out other fluids [16]. Many water sorbents have been proposed over the last decades.

Table 1: some of the best water sorbents for drying, desalination, cooling and heat storage.

Sorbent	Sorbent Type*	Application	Reference
Absorption			
[bmim][BF_4]	IL	Cooling	[17]
[emim][Ac]	IL	Cooling	[17]
[dmim][DMP]	IL	Cooling	[18]
[emim][CH_3SO_3]	IL	Drying	[18]
Adsorption			
AQSOA Z02	ZEO	Cooling/Heating	[19]
SWS-1L	CM	Cooling	[20]
Siogel	SG	Drying	[21]
NH_2-MIL-125	MOF	Heat Storage	[22]
AQSOA Z01	ZEO	Desalination	[23]

Note:* IL = Ionic Liquid; ZEO = Zeotype; CM = Composite material; SG = Silica Gel; MOF = Metal Organic Framework

Table 1 collects a summary of the best ones against their specific application. The key feature common to all the classes of sorbents in Table 1 is the possibility to tune their synthesis in order to make it optimal in a specific application. Water-sorptive inorganic salts in silica-gel [24-28] are composite sorption materials which have best represented this feature.

While inorganic salts have been widely explored, nothing is available on the water sorption characteristics of ionic liquid (IL) composites. The higher flexibility of ionic liquid synthesis as opposed to inorganic salts makes them attractive sorbents for multiple applications and can open to a totally new class of sorption composites. Working capacity is the first figure of merit to assess the potential of a sorbent working in a TSS systems. Working capacity is defined as:

$$\boldsymbol{\Delta w = w_{sorption\ state} - w_{desorption\ state}} \quad (1)$$

where $w_{sorption\ state}$ is the uptake [$g_{water}/g_{dry\ sorbent}$] of the sorbent at the sorption pressure and temperature, while $w_{desorption\ state}$ [$g_{water}/g_{dry\ sorbent}$] is the uptake in the desorption conditions of pressure and temperature. High working capacity at low regeneration temperature (<80°C) and desorption enthalpies are the main requirements in all TSS processes. Therefore, the first screening to establish whether or not a sorbent is suitable for TSS applications is on these equilibrium properties.

Adsorption desalination is an emerging TSS process evolved from adsorption heat pumps that uses low-grade heat between 60-80°C to produce pure water [29]. Its range of applications have also been recently extended for electricity generation from waste heat when coupled with reverse electrodialysis [30]. In its simplest configuration an adsorption desalinator operates according to the scheme and thermodynamic cycle described in Fig. 1.

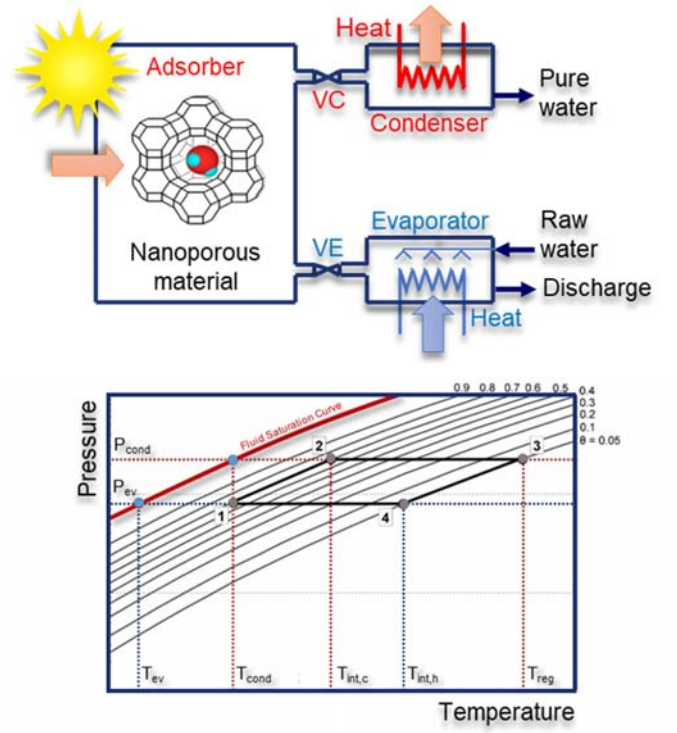

Figure 1. Working principle of an adsorption desalination process including the process block flow diagram (top) and the thermodynamic cycle (bottom). Step 1 (adsorption, states from 3 to1): valve VE is open. Valve VC is closed. Heat at ambient temperature is provided to the evaporator. Water vapor is captured in the pores of a solid nanoporous material. Valve VE is closed. Step 2 (desorption, states from 1 to 3): valve VC is open. The nanoporous material is heated up at T<100°C (regeneration). The water vapour released is condensed at ambient temperature as pure water. Note: the system operates at sub-atmospheric pressure. To run continuously the process needs of at least two alternated-operating adsorbers.

Among the nanoporous materials tested for adsorption desalination silica gel still remains the benchmark despite its limited working capacity. When regenerated at 95°C, CPO-27(Ni) metal−organic framework can achieve values of ~0.32 $g_{water}\ g_{sorbent}^{-1}$ which are higher than those of silica gel [31]. Further to physisorption in nanoporous materials, many ionic liquids (ILs) can absorb significant amounts of water at ambient temperature and release it when heated. They have been intensively investigated for heat transformation with water as refrigerant fluid [32] and drying [18]. [emim][CH_3SO_3] is a hygroscopic room temperature ionic liquid and its vapour-liquid equilibrium (VLE) with water from 20°C to 80°C has been extensively measured elsewhere [33]. Conventional investigations on VLE of ILs focus on the analysis of the activity coefficients and concerned models but lack of one significant feature that is the existence of a characteristic curve. As also observed for many nanoporous adsorbents, the Gibbs energy difference between the absorbed state and the water saturation state ($\Delta g = RT\ ln(P/P_{sat})$) is a temperature-independent curve characteristic of the particular sorbent/sorbate [34, 36]. Fig. 2 plots the characteristic curve of [emim][CH_3SO_3]/water as obtained from data of Merkel et al. [33]. This representation is most convenient to the identification of the potential of a sorption material for TSS since materials can be ranked by comparing the working capacity directly on their characteristic curve [36]. Sorption

and desorption pressure and temperatures are typical of a specific application and define two precise points of the characteristic curve. The amounts sorbed and desorbed are easily identified by reading the values corresponding to the sorption and desorption states. Fig. 1 shows the areas where sorption desalination and drying are likely to operate and highlight the significant working capacity of [emim][CH_3SO_3], well above the best performing nanoporous materials listed in Table 1. Unfortunately, utilization of pure ILs demands complex systems composed of a number of heat exchangers, mixers and separators, some ILs show corrosion issues and all these factors hinder the practical adoption of ILs in many applications [37].

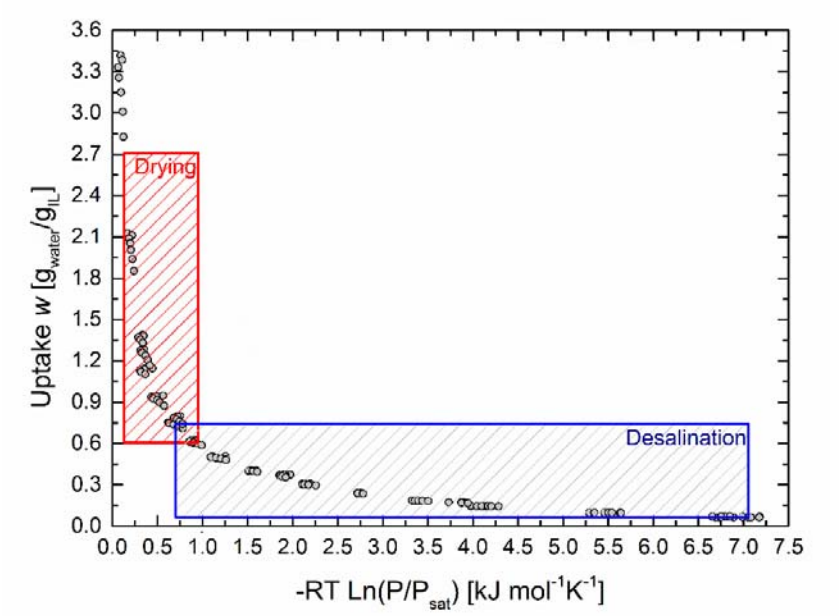

Figure 2. Characteristic curve of sorption from [emim][CH_3SO_3]/water VLE experimental data measured in [33]. Data from 20°C to 80°C collapse on a single temperature-independent curve.

These drawbacks can be avoided by structuring the IL in a nanoporous support, so eliminating the need of auxiliary equipment and mitigating eventual corrosion issues. Furthermore, the nano-confinement of IL in between charged surfaces enables the formation of preferentially oriented and self-assembled structures [38-41].
In this work we explore the water sorption equilibrium properties of the composite material [emim][CH_3SO_3] in Syloid AL-1FP silica. Initially we focus only on the IL and neglect the nanoporous support. By using classical thermodynamic absorption models, we show how the IL/water equilibrium changes in a confined state (absorption approach). Then, by using precise adsorption isotherms (adsorption approach) we show how the composite material provides a step-change in performance of sorption desalination systems and sorption drying.

2.Materials and samples preparation

1-ethyl-3-methylimidazolium methanesulfonate ionic liquid [emim][CH_3SO_3] ≥95.0% was supplied by Sigma Aldrich. Syloid AL-1FP 99.6% SiO_2 pure with properties in Table 2 was supplied by Grace and used for the nano-confinement of [emim][CH_3SO_3]. Syloid AL-1FP was dried for 12 hours at 120°C, weighed and then mixed at ambient conditions with a solution [emim][CH_3SO_3]/water at different concentrations. The mixture was then dried for 12 hours at 120°C and ambient pressure. The resulted sample was weighed to quantify the amount of

[emim][CH_3SO_3] in the Syloid AL-1FP. The degree of impregnation is indicated in percentage as mass ratio between [emim][CH_3SO_3] and whole sample**.**

Table 2: Physical properties of Syloid AL-1FP

Property		Ref.
Avarage particle size (μm)	6.5–8.1	[42]
Bulk density (g l^{-1})	566	[42]
Average Pore Volume (cm^3 g^{-1})	0.23	[43]
Average Pore Diameter (Å)	26	[43]
BET Surface Area (m^2 g^{-1})	605	[43]

3.Experimental set-up

Sorption equilibrium was measured using the Aquadyne DVS gravimetric dynamic water vapor sorption analyser (Quantachrome Instruments) with a weighing accuracy of ±1.0 μg accuracy on the weighted sample and 0.001% accuracy on suspended mass, relative humidity (RH) accuracy of ±0.8% at 20°C raising to ±1.8% at 70°C and temperature accuracy of ±0.1°C. The sample was first purged for about 12 hours under pure nitrogen flow at 25°C, in order to determine its dry weight. Then, adsorption isotherms were measured under wet nitrogen flow at 25°C for up to 20 gradual progressive stages starting from 0% RH up to 90% RH. At each relative pressure step, the temperature was kept constant until equilibrium. The steps duration was limited by 4 hours as a maximum. The equilibrium water uptake was calculated as $w = [m\,(p, T)-m_0]/m_0$ [$g_{water}/g_{dry\ sorbent}$], where m is the mass of the sample at equilibrium and m_0 is its dry mass.

4.Results and discussion

The confinement of [emim][CH_3SO_3] on a solid support enables the thermodynamic properties of the IL to be enhanced and used in a much simpler, economically convenient and viable set-up than pure IL. Fig. 3 shows the water adsorption isotherms at 25°C of [emim][CH_3SO_3] supported by Syloid AL-1FP silica (Syloid AL-1FP+[emim][CH_3SO_3]) at different values of impregnation and compares the isotherms with VLE data of [emim][CH_3SO_3] and the adsorption isotherm of Syloid AL-1FP silica, both measured on the same apparatus of composites. As common to supported IL, 60%w impregnation was the largest achievable [40].

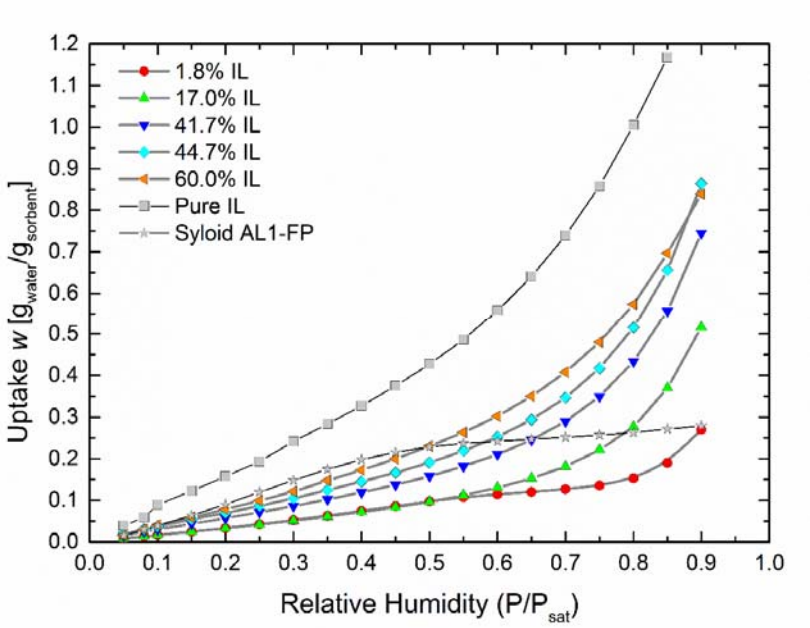

Figure 3. Water sorption isotherms at 25°C of composite Syloid AL-1FP+[emim][CH_3SO_3] at different ionic liquid concentrations, pure [emim][CH_3SO_3] and pure Syloid AL-1FP silica.

Syloid AL-1FP+[emim][CH_3SO_3] composite isotherms are upper-bounded by the pure IL isotherm, but not by the isotherm of pure Syloid AL-1FP. Water sorption in composites follows a type 3 isotherm down to 17%w impregnation, the same isotherm type of the pure IL, showing that the IL governs the sorption equilibrium. At 1.8%w impregnation, the isotherm becomes of type 2 with a shape influenced by both the Syloid AL1-FP silica support and by the pure [emim][CH_3SO_3]. Hysteresis was present on pure Syloid AL-1FP significantly decreasing by increasing the amount of impregnated ionic liquid. At 60%w impregnation adsorption and desorption was almost completely reversible, with negligible hysteresis. The comparison among the *(-Δg)* curves in Fig. 4 provides a description on how silica support and ionic liquid cooperate resulting in a special thermodynamic behavior. Moving from pure Syloid AL-1FP to the pure [emim][CH_3SO_3] a significant increase in adsorbed water at low values of *(-Δg)* is gained.

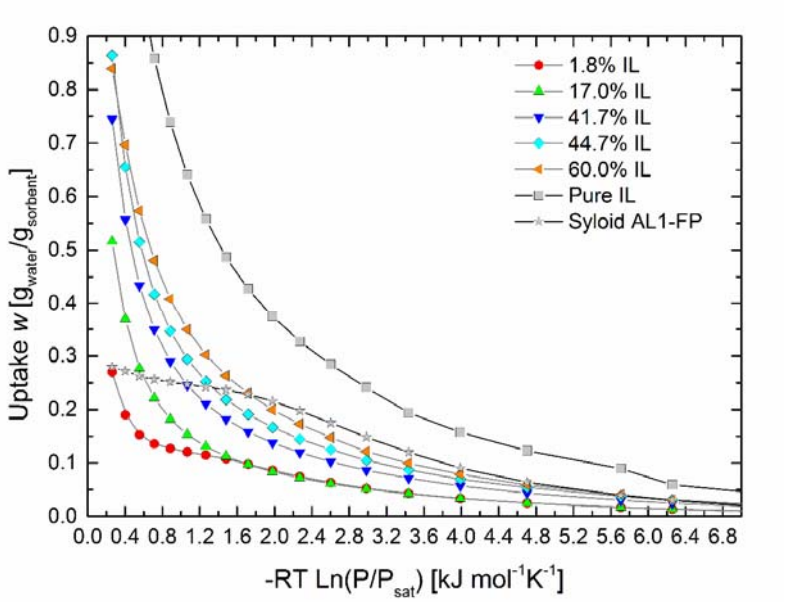

Figure 4. Characteristic curves of Syloid AL-1FP+[emim][CH_3SO_3] composite materials at different mass concentrations of impregnated ionic liquid. The figure includes also [emim][CH_3SO_3] and pure Syloid AL-1FP characteristic curves for comparison

4.1 Sorption equilibrium with Redlich-Kister excess Gibbs model

The non-random two liquid model by Renon and Prausnitz [44, 45] has been proved to be effective for the correlation of VLE of many IL/water binary systems [46-48]. In many cases, this model can be replaced by simpler excess Gibbs energy models such as the Redlich-Kister excess Gibbs model [44] which can correlate many VLE with low error [49, 50]. Therefore, the modified three-parameters Redlich-Kister (RK) model is used for the interpretation of the equilibrium of the sorption materials under investigation. Assuming Raoult law ideal solution, the molar Gibbs energy difference between the confined state and pure water at saturation is:

$$\Delta g_{P\rightarrow P_{sat}} = \Delta g_{ideal,P\rightarrow P_{sat}} + \Delta g_{ex,P\rightarrow P_{sat}} \tag{2}$$

with

$$\Delta g_{ideal,P\rightarrow P_{sat}} = R\,T\ln(x_{water}) \tag{3}$$

$$\Delta g_{ex,P\rightarrow P_{sat}} = R\,T\,x_{water}(1-x_{water})[A+B(2x_{water}-1)+C(2x_{water}-1)^2]\left[\frac{1}{1+D((2x_{water}-1))}\right] \tag{4}$$

The mole fraction x_{water} can be replaced with the uptake by using the following direct relation:

$$x_{water} = \frac{w}{w+\frac{M_w}{(1-Impr)\ M_{support}+Impr\ M_{IL}}} \tag{5}$$

where w is the uptake [$g_{water}/g_{sorbent}$], $M_{support}$ is the molecular weight of Syloid AL-1FP silica (60.08 g/mol), M_{IL} is the molecular weight of [emim][CH_3SO_3] (206.26 g/mol) and *Impr* is the weight fraction of impregnated IL in the dry Syloid AL-1FP silica.

Table 3: Parameters of the modified Redlich-Kister excess Gibbs energy model (eq. (4)) for water sorption in pure [emim][CH_3SO_3], composite material Syloid AL-1FP+[emim][CH_3SO_3] and pure Syloid AL-1FP silica.

	Impr	A	B	C	D
100% [emim][CH_3SO_3]	1.000	-6.442	4.379	0.189	0.000
40.0%Syloid AL-1FP+60.0%[emim][CH_3SO_3]	0.600	-9.217	5.575	2.853	1.002
58.3%Syloid AL-1FP+41.7.0%[emim][CH_3SO_3]	0.417	-0.185	1.643	-0.078	0.983
83.0%Syloid AL-1FP+17.0%[emim][CH_3SO_3]	0.170	1.594	0.278	-0.930	0.992
98.2%Syloid AL-1FP+1.8%[emim][CH_3SO_3]	0.018	2.782	1.441	-0.465	1.011
100% Syloid AL-1FP	0.000	2.430	12.380	11.556	0.982

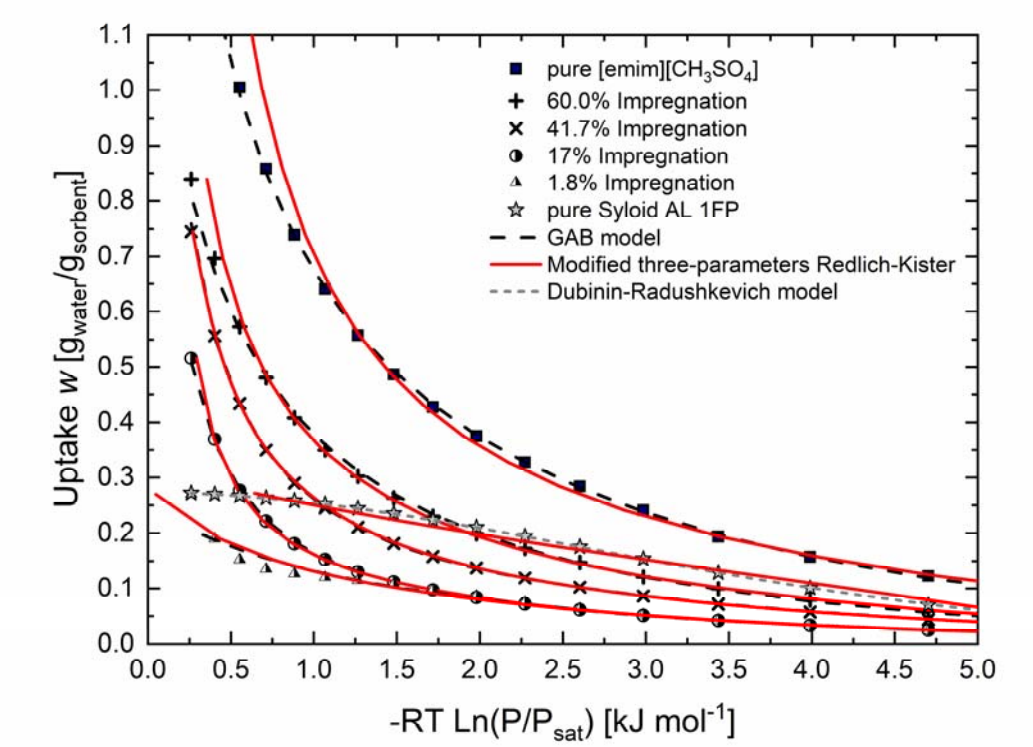

Figure 5. Correlation of Gibbs energy change from experimental data with modified three-parameters Redlich-Kister excess Gibbs energy model (parameters in Table 3), GAB isotherm model (parameters in Table 5) and Dubinin-Radushkevich model (only for pure Syloid AL-1FP silica).

As shown in Fig. 5, the RK model provides an adequate representation of VLE data of [emim][CH_3SO_3]/water and adsorption equilibrium of Syloid AL-1FP+[emim][CH_3SO_3]/water down to 1.8% impregnation. For 98.2%Syloid AL-1FP+1.8%[emim][CH_3SO_3] and pure Syloid AL-1FP, the RK model is inadequate with maximal average deviations of 30% and 12%. Table 2 reports the model parameters which show a trend, dependent on the amount of IL impregnated. The nano-confinement of the IL increases the correlation between temperature and concentration. For pure IL this correlation can be based on a two-parameters Redlich-Kister model (coefficient D is unnecessary and C has a low value) while for the composite material only a four parameters

model can fit the data adequately. Parameters C and D enable a stronger non-linear interaction between the temperature-dependent ratio (P/P_{sat}) and the right hand side of eq. (2) which is instead concentration-dependent. This effect has a direct consequence on the operating conditions of thermally-driven technologies that can benefit of a larger concentration swing (or working capacity) at moderate temperature swing and viceversa.

4.2 Increased temperature sensitivity of nano-confined ionic liquid

The [emim][CH_3SO_3]/water VLE is described by the equality of the chemical potential of water in vapor and liquid phase. By assuming negligible amount of ionic liquid in vapor phase, a single equation is representative of the VLE:

$$\boldsymbol{x_{water}} = \frac{\mathbf{1}}{\boldsymbol{\gamma_{water}}} \frac{\boldsymbol{P}}{\boldsymbol{P_{sat,water}}} \tag{6}$$

or

$$\boldsymbol{a_{water}} = \frac{\boldsymbol{P}}{\boldsymbol{P_{sat,water}}} \tag{7}$$

where x_{water} is the mole fraction of water in the liquid phase, γ_{water} is the activity coefficient of water in the IL-rich phase, $P_{sat,water}$ is the saturation pressure of water at the equilibrium temperature, P is the pressure of water in the vapour phase and $a_{water} = x_{water}\,\gamma_{water}$ is the activity of water in the IL-rich phase. The ratio ($P/P_{sat,water}$) is the relative humidity (RH). In a large number of applicative cases, the thermodynamic equilibrium is more conveniently expressed in terms of uptake of water w [$g_{water}/g_{sorbent}$] instead of mole fraction x_{water}. If only the IL is considered in the equilibrium, mole fraction can be converted in uptake by the following direct correlation:

$$\boldsymbol{x_{water}} = \frac{\boldsymbol{w}}{\boldsymbol{w}+\frac{\boldsymbol{M_W}}{\boldsymbol{M_{IL}}}} \tag{8}$$

where w is the uptake [g_{water}/g_{IL}], M_w is the molecular weight of water and M_{IL} is the molecular weight of the IL. It is worth stressing that the analysis of the equilibrium of pure IL and IL in composite material with eq. (6) and eq. (8) takes into account only the amount of impregnated IL and neglects the presence of the silica support. The trend of the activity coefficient of water in the IL rich-phase vs relative humidity (Fig. 6) is non-linear and depends on temperature only through the water saturation pressure. In fact, the activity coefficients at 20°C are essentially aligned with those at 80°C. The following simple correlation can describe the experimental activity coefficients:

$$\boldsymbol{\gamma} = \left(\frac{\boldsymbol{P}}{\boldsymbol{P_s}}\right)^{\boldsymbol{\alpha}} \tag{9}$$

where α is a coefficient ranging between 0 and 1. Eq. (9) is a simple basis to compare the equilibrium of materials with different impregnations and is able to capture the activity coefficient trends with acceptable error.

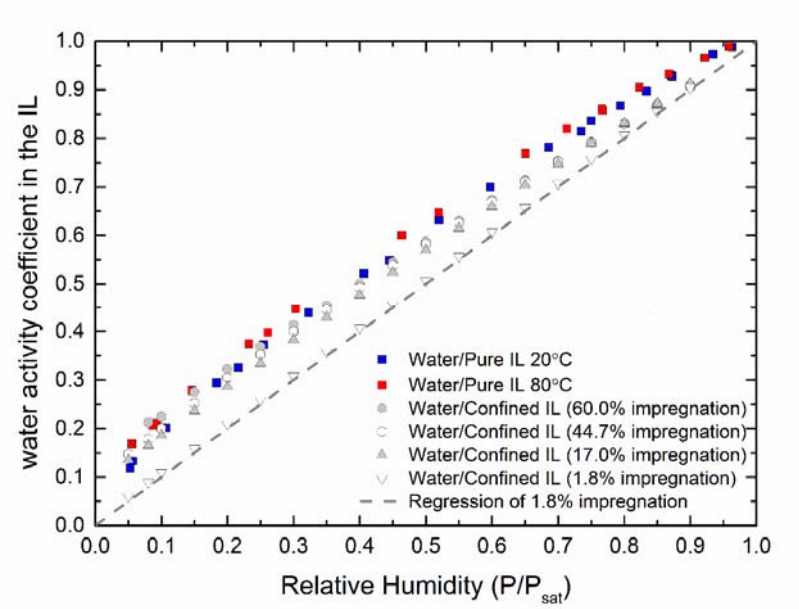

Figure 6. Experimental water sorption activity coefficient on pure [emim][CH_3SO_3] at 20°C and 80°C and on Syloid AL-1FP+[emim][CH_3SO_3] composites at different impregnations.

Table 4: values of α parameter in eq. (9) at 20°C.

Sorbent	α
Pure [emim][CH_3SO_3]	0.68
40.0%Syloid AL-1FP+60.0%[emim][CH_3SO_3]	0.68
44.7%Syloid AL-1FP+55.3%[emim][CH_3SO_3]	0.72
83.0%Syloid AL-1FP+17.0%[emim][CH_3SO_3]	0.77
98.2%Syloid AL-1FP+1.8%[emim][CH_3SO_3]	0.97

α coefficients of Table 4 decrease progressively from 1 to 0.68 at 60% impregnation, this is the same α value of non-confined IL. Therefore, at 60% impregnation the composite material has water sorption equilibrium very similar to the bulk IL, while by decreasing the concentrations below 60% the interaction between IL and support material is more and more significant. Fig. 7 shows a comparison between bulk liquid [emim][CH_3SO_3] and in 40%Syloid AL-1FP+60%[emim][CH_3SO_3] composite in terms of water activities. Water activity curves at 25°C and 80°C of the bulk [emim][CH_3SO_3] are essentially identical, while for 40%Syloid AL-1FP+60%[emim][CH_3SO_3] the curves are well distinct, suggesting that the composite sorbent will have higher sensitivity to temperature changes than the non-confined IL, therefore larger decrease in water content on heating.

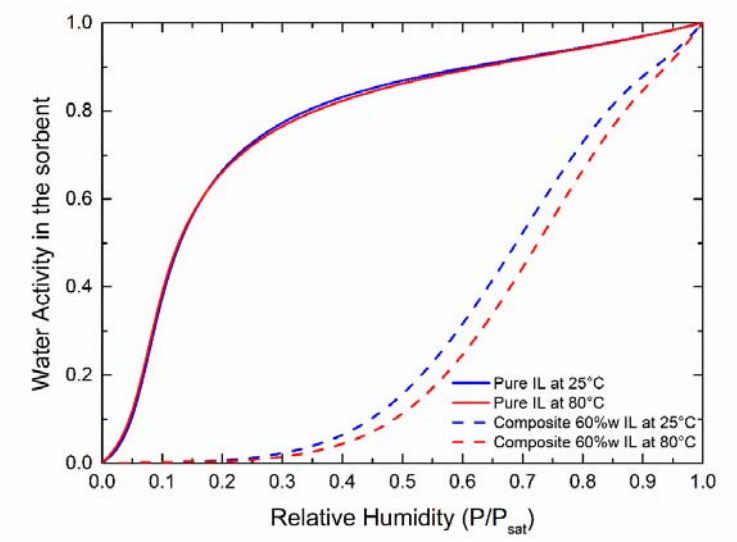

Figure 7. Activity of water in bulk [emim][CH_3SO_3] and nano-confined [emim][CH_3SO_3] at 25°C and 80°C. The activity is computed in this case by including also the silica support weight (eq. (5)).

4.3 Application of silica-supported [emim][CH_3SO_3] ionic liquid to desalination and drying

Gibbs excess models are useful to capture the change of thermodynamic behavior of the IL between confined and non-confined state but have limits in representing accurately the experimental data. Adsorption isotherms can overcome this limitations by enabling a more precise fitting and allowing therefore unequivocal assessment of the potential of the materials when used in desalination and drying applications. Type 3 isotherms of Fig. 3 are excellently described by the Guggenheim-Anderson-de Boer (GAB) model [51]:

$$\mathbf{w} = \mathbf{w}_{\boldsymbol{m}} \frac{\boldsymbol{C}\,\boldsymbol{K}\left(\frac{\boldsymbol{P}}{\boldsymbol{P_s}}\right)}{\left(\mathbf{1}-\boldsymbol{K}\frac{\boldsymbol{P}}{\boldsymbol{P_s}}\right)\left(\mathbf{1}-\boldsymbol{K}\frac{\boldsymbol{P}}{\boldsymbol{P_s}}+\boldsymbol{C}\,\boldsymbol{K}\frac{\boldsymbol{P}}{\boldsymbol{P_s}}\right)} \tag{10}$$

where w_m [$g_{water}/g_{sorbent}$] is the water content corresponding to monolayer saturation, C is the Guggenheim constant and K is a correction factor of the monolayer adsorption. In Fig. 5, a comparison between model prediction and experimental characteristic curves is presented with parameters reported in Table 5. Adsorption of water on pure Syloid AL-1FP follows a type 1 isotherm and it is precisely described by Dubinin-Radushkevich isotherm:

$$-\boldsymbol{RT}\ln\left(\frac{\boldsymbol{P}}{\boldsymbol{P_s}}\right) = \mathbf{E}\left[-\boldsymbol{ln}\left(\frac{\boldsymbol{w}}{\boldsymbol{w_o}}\right)\right]^{\mathbf{1}/\boldsymbol{n}} \tag{11}$$

where E=227.80 kJ/kg is the characteristic energy of adsorption, w_0=0.267 $g_{water}/g_{sorbent}$ is the saturation capacity of the material and n=2 is a regression constant. The comparison between the two approaches in Fig. 4 shows GAB isotherm providing the best interpretation of sorption equilibrium, although the RK model allows also to address non-type 3 isotherms such in the case of 98.2%Syloid AL-1FP+1.8%[emim][CH_3SO_3] and pure Syloid AL-1FP. Fig. 8 reports the results of calculation on the adsorption desalination [11, 52] and drying ideal cycles.

In the operational regions highlighted in Fig. 1, 40%Syloid AL-1FP+60% [emim][CH_3SO_3] (SIL) is able to achieve the highest working capacity among all the tested impregnations. When assessed against Siogel silica gel, the material presently suggested for adsorption desalination and drying in wet appliances, the performance of allows a step-change in performance.

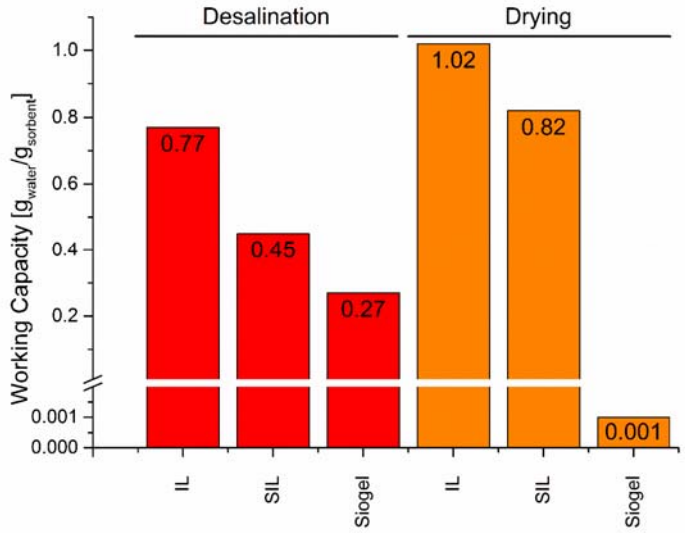

Figure 8. Working capacities of pure [emim][CH_3SO_3] (pure IL), 40.0%Syloid AL-1FP+60.0%[emim][CH_3SO_3] (SIL) and Siogel silica gel in desalination and drying. Sorption and desorption conditions are calculated by assuming a sorption processes [11, 22, 47, 48] working at the following conditions: Desalination sorption: (T_{sorpt}=25°C, RH_{sorpt}=0.75); Desalination desorption: ($T_{MAX,desorpt}$=80°C, $RH_{desorpt}$=0.09); Drying sorption: (T_{sorpt}=25°C, RH_{sorpt}=0.95); Drying desorption: ($T_{desorpt}$=50°C, $RH_{desorpt}$=0.70).

Table 5: Parameters of GAB isotherm model (eqn. (10)) for water sorption in pure [emim][CH_3SO_3], composite material Syloid AL-1FP+[emim][CH_3SO_3].

	w_m [$g_{water}/g_{sorbent}$]	C	K
100% [emim][CH_3SO_3]	0.384	2.562	0.843
40.0%Syloid AL-1FP+60.0%[emim][CH_3SO_3]	0.248	1.763	0.826
58.3%Syloid AL-1FP+41.7%[emim][CH_3SO_3]	0.111	3.092	0.957
83.0%Syloid AL-1FP+17.0%[emim][CH_3SO_3]	0.070	2.613	0.965
98.2%Syloid AL-1FP+1.8%[emim][CH_3SO_3]	0.153	1.923	0.564

Clean water production in adsorption desalination systems is 1.7 times more than conventional Siogel silica gel and drying can be achieved at operating conditions where conventional Siogel silica gel does not operate. When compared with the performance of pure IL, composite SIL material has working capacity higher than 60% the working capacity of pure IL in drying. This is achieved thanks to the confinement of IL in the nanopores of the silica support.
An additional advantage of the SIL composite against conventional silica gels consists of its higher volumetric working capacity. As shown by Table 6, smaller adsorption beds are possible when the SIL is used, with a beneficial expected impact on the capital investment of adsorption desalination

systems. By allocating one third of the capital cost of to the adsorbers, the composite material allows 50% smaller elements than Silica gel A++. On the basis of the costs of $108k reported elsewhere for a 1000 $kg_{adsorbent}$ desalination system [29], the utilization of the SIL material can enable reduction of the capital cost of ~20%. This improve further an already economically attractive technology such as adsorption desalination [53, 54]. However, this benefit requires further and more detailed assessment since it can be counterbalanced by a cost of the composite higher than silica gel.

Table 6: Comparison among silica gels and composite supported ionic liquid on water storage density

	Apparent density kg/m^3	Gravimetric working capacity $kg_{water}/kg_{sorbent}$	Volumetric working capacity $kg_{water}/m^3_{sorbent}$	Ref.
Silica Gel Siogel	735	0.36	265	[30]
Silica Gel Type A++	730	0.44	321	[30]
Silica Gel RD 2560	800	0.30	240	[30]
40.0%Syloid AL-1FP+60.0%[emim][CH_3SO_3]	850*	0.73	621	measured

*the value corresponds to manually compacted powder.

5. Conclusions

Water sorption equilibria of pure and composite materials made of 1-ethyl-3-methylimidazolium methanesulfonate and Syloid AL-1F silica have been investigated at different mass concentrations of 1-ethyl-3-methylimidazolium methanesulfonate in the silica support. Type 3 sorption isotherm, typical of 1-ethyl-3-methylimidazolium methanesulfonate/water vapor-liquid equilibrium is maintained at concentrations of impregnated 1-ethyl-3-methylimidazolium methanesulfonate down to 17%w. Both the Guggenheim-Anderson-de Boer adsorption isotherm model and the Redlich-Kister excess Gibbs energy model provide an appropriate description of the equilibria. However, Redlich-Kister excess Gibbs energy model fits with variable errors different types of isotherms while Guggenheim-Anderson-de Boer fits excellently only type 3 isotherm data. The confinement IL in the silica nanopores results in larger water produced upon heating than when the IL is in bulk state. This is a beneficial feature for temperature swing adsorption technologies such as adsorption desalination and drying. The optimal SIL material is composed of 40%w Syloid AL-1FP and 60%w 1-ethyl-3-methylimidazolium methanesulfonate and enables the production of 1.7 times more pure water than the currently used nanoporous sorbents. In drying applications, SIL material can be regenerated at 50°C, a temperature level at which conventional drying materials do not work.

Acknowledgment

The research leading to these results has received funding from the EPSRC “Micro-scale energy storage for super-efficient wet appliances” project EP/P010954/1.

References

[1] N. Stern, The Criticality of the Next 10 Years: Delivering the Global Agenda and Building Infrastructure for the 21st Century, The Royal Society, 28th October 2016.
[2] J. A. Wurzbacher, C. Gebald and A. Steinfeld, Energy Environ. Sci., 2011, 4, 3584–3592.
[3] L. Huber, P. Ruch, R. Hauert, S. Kumar Matam, G. Saucke, S. Yoon, Y. Zhang and M. M. Koebel, RSC Adv., 2016, 6, 80729–80738.
[4] F. Jeremias, V. Lozan, S.K. Henninger and C. Janiak, Dalton Trans., 2013, 42, 15967–15973.

[5] N. Yu, R.Z. Wang and L.W. Wang, Prog. Energy Combust. Sci., 2013, 39, 489–514.
[6] M.M. Tokarev, L.G. Gordeeva, A.D. Grekova and Y.I. Aristov, Appl. Energy, 2018, 211, 136–145.
[7] F. Jeremias, D. Fröhlich, C. Janiak and S.K. Henninger, NewJ.Chem., 2014, 38, 1846.
[8] F. Ziegler, Int. J. Refrig., 2009, 32, 566-576.
[9] S.K. Henninger, H.A. Habib and C. Janiak, J. Am. Chem. Soc., 2009, 131, 2776–2777.
[10] A.D. Grekova, L.G. Gordeeva, Z. Lu, R. Wang and Yuri I. Aristov, Sol. Energy Mat. Sol. C., 2018, 176, 273–279.
[11] M.W. Shahzad, K.C. Ng and K. Thu, Environ. Sci.: Water Res. Technol., 2016, 2, 206–212.
[12] K.C. Ng, I.I. El-Sharkawy, B.B. Saha and A. Chakraborty, Adsorption Desalination: A Novel Method. In: Wang L.K., Chen J.P., Hung YT., Shammas N.K. (eds) Membrane and Desalination Technologies, 2011, Handbook of Environmental Engineering, vol 13. Humana Press, Totowa, New York.
[13] J.C. Atuonwu, G. van Straten, H.C. van Deventer and A. J. B. van Boxtel, Dry. Technol., 2011, 29, 12, 1459–1471.
[14] Y.D. Tu, R.Z. Wang and T.S. Ge, Energy Convers. Manage., 2018, 156, 568–574.
[15] J.A. Mason, K. Sumida, Z.R. Herm, R. Krishna and J.R. Long, Energy Environ. Sci., 2011, 4, 3030-3040.
[16] G. Santori and C.D. Santis, Sust. Mat. Technol., 2017, 12, 52–61.
[17] D.B. Boman, D.C. Hoysall, M.A. Staedter, A.G. Mikko, J. Ponkala and S. Garimella, Int. J. Refrig., 2017, 77, 149–175.
[18] D. Zheng, L. Dong, W. Huang, X. Wu and N. Nie, Renew. Sust. Energy Rev., 2014, 37, 47–68.
[18] M.K. Krannich, F. Heym and F. Jess, J. Chem. Eng. Data, 2016, 61, 1162−1176.
[19] A. Freni, B. Dawoud, L. Bonaccorsi, S. Chmielewski, A. Frazzica, L Calabrese and G. Restuccia, Characterization of Zeolite-Based Coatings for Adsorption Heat Pumps, Springer International Publishing, 2015.
[20] G. Restuccia, A. Freni, S. Vasta and Y. Aristov, Int. J. Refrig., 2004, 27, 3, 284-293.
[21] G. Santori, A. Frazzica, A. Freni, M. Galieni, L. Bonaccorsi, F. Polonara and G. Restuccia, Energy, 2013, 50, 170–176.
[22] L.G. Gordeeva, M.V. Solovyeva and Y.I. Aristov, Energy, 2016, 100, 18–24.
[23] S. Kayal, S. Baichuan and B.B. Saha, Int. J. Heat Mass Tran., 2016, 92, 1120–1127.
[24] Y. Aristov, G. Restuccia, G. Cacciola and V.N. Parmon, Appl. Therm. Eng., 2002, 22, 191–204.
[25] Y. Aristov, M.M. Tokarev, G. Cacciola and G. Restuccia, React. Kinet. Catal. L., 1996, 59, 325–333.
[26] Y. Aristov, Appl. Therm. Eng., 2013, 50, 1610-1618.
[27] A.D. Grekova, I.S. Girnik, V.V. Nikulin, M.M. Tokarev, L.G. Gordeeva and Y. Aristov, Energy, 2016, 106, 231–239.
[28] I. Glaznev, I. Ponomarenko, S. Kirik and Y. Aristov, Int. J. Refrig., 2011, 34, 1244–1250.
[29] K.C. Ng, K. Thu, Y. Kim, A. Chakraborty and G. Amy, Desalination, 2013, 308, 161−179.
[30] C. Olkis, G. Santori and S. Brandani, Appl. Energy, 2018, 231, 222−234.
[31] E. Elsayed, R. Al-Dadah, S. Mahmoud, P. A. Anderson, A. Elsayed and P. G. Youssef, Desalination, 2017, 406, 25−36.
[32] R. Kühn, J. Römer and F. Ziegler, Int. J. Refr., 2018, in press. https://doi.org/10.1016/j.ijrefrig.2018.07.019

[33] M. Merkel, C. Weber, M. Faust and K. Schaber, Fluid Phase Equilibr., 2015, 394, 29–37.
[34] M. Polanyi, T. Faraday Soc., 1932; 28, 316–33.
[35] M.M. Dubinin, Chem. Rev., 1960, 60, 235–241.
[36] Yu. Aristov, Appl. Therm. Eng., 2014, 72, 166-175.
[37] P. Wasserscheid and M. Seiler, ChemSusChem, 2011, 4, 459–463.
[38] U. Shafique, V. Dorn, A. Paschke and G. Schüürmann, Chem. Commun., 2017, 53, 589–592.
[39] R. Futamura, T. Iiyama, Y. Takasaki, Y. Gogotsi, M. Biggs, M. Salanne, J. Ségalini, P. Simon and K. Kaneko, Nat. Mater., 2017, 16, 1225-1232.
[40] R. Fehrmann, A. Riisager and M. Haumann, Supported Ionic Liquids: Fundamentals and Applications, 2014 Wiley-VCH Verlag GmbH & Co., KGaA, Boschstr. 12, 69469 Weinheim, Germany.
[41] S. Perkin, L. Crowhurst, H. Niedermeyer, T. Welton, A. M. Smith and N. Nand Gosvami, Chem. Comm., 2011, 47, 6572–6574
[42] T. Hussain, L. J. Waters, G. M. B. Parkes and Y. Shahzad, Colloids Surf. A: Physicochem. Eng. Aspects 2017, 520, 428–435.
[43] Talib Hussain, The application of microwave formulation and isothermal titration calorimetry for pharmaceutical compounds. Doctoral thesis, University of Huddersfield, 2014.
[44] J. M. Prausnitz, R.N. Lichtenthaler, E.G. de Azevedo, Molecular Thermodynamics of Fluid Phase equilibria, Third Edition, Pearson Education, 1988.
[45] H. Renon and J.M. Prausnitz, AIChE J., 1968, 14, 135–144.
[46] C. Römich, N.C. Merkel, A. Valbonesi, K. Schaber, S. Sauer and T.J.S. Schubert, J. Chem. Eng. Data, 2012, 57, 2258–2264.
[47] N.C. Merkel, C. Römich, R. Bernewitz, H. Künemund, M. Gleiß, S. Sauer, T.J.S. Schubert, G. Guthausen and K. Schaber, J. Chem. Eng. Data, 2014, 59, 560–570.
[48] R. Kato, M. Krummen and J. Gmehling, Fluid Phase Equilib., 2004, 224, 47–54.
[49] M. Królikowska, K. Paduszyński, M. Królikowski, P. Lipiński and J. Antonowicz, Ind. Eng. Chem. Res., 2014, 53, 18316–18325.
[50] M. Królikowska and M. Zawadzki, J. Mol. Liq., 2018, 249, 153–159.
[51] C.M. Samaniego-Esguerra, I.F. Boag and G.L. Robertson, J. Food Eng., 1991, 13, 115–133.
[52] J.W. Wu, M.J. Biggs, P. Pendleton, A. Badalyan, E.J. Hu, Appl. Energy, 2012, 98, 190–197.
[53] N. Ghaffour, T. M. Missimer, G. L. Amy, Desalination, 2013, 309, 197–207.
[54] S. Sadri, M. Ameri, R. Haghighi Khoshkhoo, Desalination, 2018, 428, 69–75.